Chinese Chemical Letters 37 (2026) 111533

Contents lists available at ScienceDirect

Chinese Chemical Letters

journal homepage: www.elsevier.com/locate/cclet

Organic liquid electrolyte for low-temperature sodium-ion batteries

Xiaosa Zhang[a,b,c,d], Shanghao Zhou[b,c,d], Xiaomin Chen[a,b,c,d], Xu Xu[a,b,c,d], Xiaoyan Shi[a,b,c,d], Zhiming Zhou[a,b,c,d], Yun Wan[a,b,c,d], Xinhui Zeng[a,b,c,d], Xunzhu Zhou[b,c,d,e,*], Xiang Chen[f], Shu-Lei Chou[a,b,c,d,*], Lin Li[a,b,c,d,*]

[a] Institute for Carbon Neutralization Technology, College of Chemistry and Materials Engineering, Wenzhou University, Wenzhou 325035, China
[b] Zhejiang Provincial Key Laboratory of Advanced Battery Materials and Technology, Wenzhou University Technology Innovation Institute for Carbon Neutralization, Wenzhou 325035, China
[c] Zhejiang-Australia International Joint Laboratory for Sodium-Ion Batteries, Wenzhou University Technology Innovation Institute for Carbon Neutralization, Wenzhou 325035, China
[d] Wenzhou Key Laboratory of Sodium-Ion Batteries, Wenzhou University Technology Innovation Institute for Carbon Neutralization, Wenzhou 325035, China
[e] Institute School of Materials Science and Engineering, Key Laboratory of Structure and Functional Regulation of Hybrid Material (Ministry of Education), Anhui University, Hefei 230601, China
[f] College of Textile Science and Engineering (International Institute of Silk), Zhejiang Sci-Tech University, Hangzhou 310018, China

ARTICLE INFO

Article history:
Received 29 May 2025
Revised 29 June 2025
Accepted 2 July 2025
Available online 3 July 2025

Keywords:
Sodium-ion batteries
Low temperature
Organic liquid electrolyte
Charge transfer kinetics
Electrochemical performance

ABSTRACT

Low-temperature energy storage technology plays a crucial role in sustaining energy supply for interstellar exploration, polar research stations, military facilities in extremely cold regions. Sodium-ion batteries (SIBs) are regarded as potential candidates for large-scale energy storage systems under extreme low-temperature conditions due to their abundant sodium resources, low cost and superior temperature tolerance. As a critical component of SIBs, the electrolyte is closely related to the charge transfer kinetics within the battery and significantly influences its low-temperature electrochemical performance. Herein, we present a comprehensive review focusing on recent advances in organic liquid electrolytes for enhancing the low-temperature performance of SIBs. Firstly, the failure mechanisms of SIBs at low temperatures are systematically analyzed from the perspective of charge transfer kinetics. Subsequently, the electrolyte design strategies for low-temperature SIBs are introduced based on two evaluation dimensions: half cell and full cell systems. Finally, the future research directions for developing advanced electrolytes to improve the low-temperature performance of SIBs are proposed. This review provides valuable insights into electrolyte optimization strategies, which are expected to accelerate the development of high-performance SIBs for reliable energy storage in extreme cold environments.

© 2026 Published by Elsevier B.V. on behalf of Chinese Chemical Society and Institute of Materia Medica, Chinese Academy of Medical Sciences.

1. Introduction

With increasing exploration of extreme low-temperature environments, the development of low-temperature energy storage technology has become a strategic research direction in the field of energy science (Fig. 1a) [1–3]. For interstellar exploration, low-temperature energy storage systems play a pivotal role in meeting the energy demands of deep-space missions, enabling the long-term space habitation and utilization of extraterrestrial resources [4,5]. Meanwhile, polar research stations, military facilities in cold regions, and high-latitude cities require low-temperature energy storage devices to ensure stable energy supply for their infrastructure. However, the traditional energy storage technologies suffer from severe performance degradation at low temperature, making them struggle to meet practical application demands [6,7]. Therefore, the development of high-performance low-temperature energy storage technology holds crucial practical significance for supporting humanity's exploration of unknown frontiers and achieving stable energy supply in extreme low-temperature environments.

Lithium-ion batteries (LIBs), as a typical electrochemical energy storage technology, have been widely applied in various fields of daily life, including portable electronic devices and electric vehicles [8–10]. However, the limited and unevenly distributed lithium resources, along with unsatisfactory low-temperature performance, inevitably hinder the application of LIBs for energy storage in extreme low-temperature environments [11–14]. Recently, sodium-ion batteries (SIBs) have emerged as a vital complementary technology to LIBs for large-scale energy storage systems, driven by

* Corresponding authors.
E-mail addresses: xunzhuzhou@ahu.edu.cn (X. Zhou), chou@wzu.edu.cn (S.-L. Chou), linli@wzu.edu.cn (L. Li).

https://doi.org/10.1016/j.cclet.2025.111533
1001-8417/© 2026 Published by Elsevier B.V. on behalf of Chinese Chemical Society and Institute of Materia Medica, Chinese Academy of Medical Sciences.

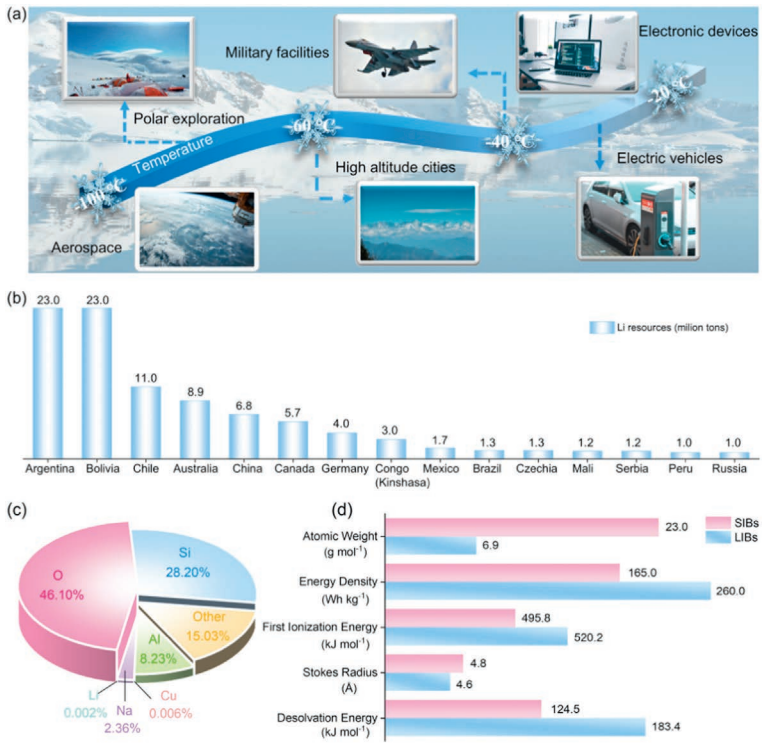


Fig. 1. (a) Potential future applications of low-temperature SIBs. (b) Global distribution of identified lithium resources at the end of 2024. All locations with at least one million tons are indicated; collectively accounting for 98 % of the global total. (c) Crustal element abundance. (d) Comparative analysis of critical performance characteristics of LIBs and SIBs.

the abundance of sodium resources and their lower manufacturing costs (Figs. 1b and c) [15–17]. In addition, sodium exhibits no reactivity with aluminum, the substitution of copper with aluminum as the anode current collector becomes feasible, thereby significantly reducing the overall cost of SIBs. More importantly, as shown in Fig. 1d, Na^+ endows weaker Lewis acidity and smaller Stokes radius compared to Li^+ (4.6 *vs.* 4.8 Å), enabling higher ionic conductivity of sodium-based electrolytes [18,19]. Furthermore, the desolvation energy of Na^+ is approximately 25 %–30 % lower than that of Li^+ in commonly used organic solvent systems, which significantly accelerates the interfacial charge transfer kinetics [20,21]. Benefiting from these unique advantages, SIBs are expected to exhibit superior low-temperature electrochemical performance, making them as an ideal candidate technology for large-scale energy storage systems in extreme cold environments [22,23].

Under extreme low-temperature conditions, the charge transfer kinetics of SIBs deteriorates significantly, leading to severe degradation of electrochemical performance [24]. As the critical components of SIBs, electrode materials and electrolytes are closely related to the charge transfer kinetics, thereby profoundly influencing the low-temperature performance [25,26]. Recent advances in structural and morphological engineering have significantly enhanced the low-temperature sodium storage performance of electrode materials [27–29]. However, elaborately engineered electrodes and novel electrode materials often involve complex and costly preparation processes, unavoidably limiting their widespread application [11]. Electrolyte, serving as the “blood” of SIBs, governs Na^+ migration, desolvation processes, and interfacial ion transport behavior [30]. Additionally, the composition of electrolytes is highly tunable, requiring no intricate manufacturing processes and having minimal impact on subsequent battery manufacturing. Thus, developing high-performance low-temperature electrolytes is of great significance for promoting the extreme low-temperature application of SIBs [31,32].

To date, various electrolytes have been explored for low-temperature SIBs, including aqueous electrolytes [33], organic liquid electrolytes [34,35], ionic liquid electrolytes [36] and solid-state electrolytes [37]. Although aqueous electrolytes feature high safety, environmentally friendly, high ionic conductivity and low cost, the narrow electrochemical window and high freezing point limit their practical application [38]. Ionic liquids possess inherent advantages of excellent thermal stability, non-flammability and wide electrochemical windows, but suffer from high viscosity, low ionic conductivity and high cost [39]. Solid-state electrolytes are regarded as promising candidates for high-energy-density SIBs due to their high safety, wide electrochemical windows and superior thermal stability. However, the limited ionic conductivity and poor interfacial contact inevitably hinder their application at low temperature conditions [40]. Noticeably, organic liquid electrolytes with the advantages of high ionic conductivity, excellent permeability and low freezing point are considered as the most promising candidates for low-temperature SIBs [41–43]. To the best of our knowledge, however, limited attention has been given to systematically summarize recent achievements in organic liquid electrolytes for low-temperature SIBs.

In this review, we are committed to summarizing the recent advancements in organic liquid electrolytes for enhancing the low-temperature performance of SIBs. Firstly, we systematically analyze the failure mechanisms of low-temperature SIBs from a charge transfer kinetic perspective. Subsequently, we comprehensively review recent achievements in low-temperature SIBs electrolyte design over the past few years, covering both half cell and full cell configurations. Finally, we propose future research directions for low-temperature SIBs electrolytes. This review aims to provide meaningful guidance for the rational design of electrolytes tailored for low-temperature SIBs, thereby advancing their energy storage applications in extreme cold environments.

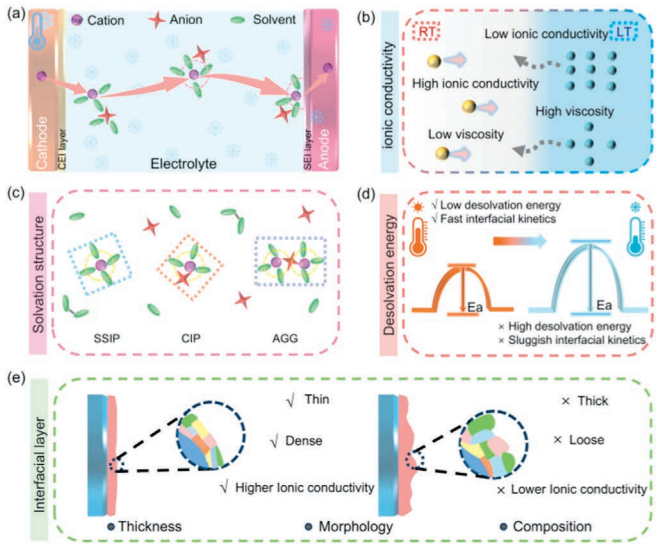


Fig. 2. (a) Illustration of four stages of Na^+ transfer during the charge process. (b) Changes in ionic conductivity and viscosity at low temperature. (c) Three typical inner Na^+ solvation structure at low temperature. (d) Evolution of desolvation energy barrier during temperature decreases. (e) Three main concerns of the EEI layer.

2. Failure mechanism of low-temperature SIBs from the perspective of kinetics

As the operation temperature decreases, interfacial charge transfer kinetics decreases significantly, resulting in low reversible capacity, large overpotential, poor rate performance and low energy density [44,45]. Meanwhile, the sluggish charge transfer kinetics induces sodium deposition behavior at anode surface, leading to several safety issues and fast capacity degradation [46]. In general, the failure mechanism of SIBs at low temperature is mainly related to the following four charge transfer kinetics process (Fig. 2a) [47]: (1) Diffusion of solvated Na^+ through electrolyte bulk phase towards electrode interface. Ionic conductivity (σ), viscosity (η) and freezing point play key role on Na^+ transport kinetics in electrolytes. As the temperature decreases, the viscosity of electrolyte increases, and the ionic conductivity declines, resulting in sluggish diffusion of solvated Na^+ (Fig. 2b) [48,49]. (2) Desolvation process at the electrode/electrolyte interface (EEI). As shown in Fig. 2c, Na^+ usually exists as solvated ions in electrolytes, which can form three different solvated structures based on Na^+-solvent interactions, including solvent separated ion pairs (SSIPs), contact ion pairs (CIPs) and aggregates (AGGs) [50]. However, the storage of Na^+ in electrode materials generally requires fully desolvated Na^+. As the temperature decreases, the desolvation energy barrier of Na^+ in bulk electrolyte increases significantly, which inevitably results in unsatisfied low-temperature sodium storage performance (Fig. 2d) [51,52]. (3) Transport of Na^+ across the electrode/electrolyte interface. The ion transport properties of EEI films are mainly determined by their chemical composition and microstructure. Noticeably, thin EEIs with fast ion-conducting characters are more conducive for the rapid transport of Na^+ across the interface (Fig. 2e) [31,53]. (4) Transfer of Na^+/e^- within the electrode materials. Electrode materials with high ionic and electronic conductivity can significantly enhance charge transfer kinetics, thereby improving the low-temperature performance of SIBs [54,55].

To date, researchers have improved the ionic/electronic conductivity by optimizing the structure and morphology of electrode materials, which effectively enhance the low-temperature performance of SIBs [56]. Electrolyte, as a core component of SIBs, is closely associated with three critical stages of Na^+ transport kinetics (bulk electrolyte ionic conduction, Na^+ desolvation process, and interfacial Na^+ transport), directly determining the low-temperature performance of batteries [57]. However, current research on electrolytes for low-temperature SIBs remains in its early stages. Therefore, systematically summarizing the recent advancements in low-temperature electrolytes is of great significance for advancing the energy storage applications of SIBs in low-temperature scenarios.

3. Recent achievement of electrolyte design for low-temperature SIBs

To advance SIBs applications in extreme low-temperature environments, an ideal electrolyte must simultaneously fulfill the following requirements: (1) Possessing high ionic conductivity and ultra-low freezing point to maintain rapid Na^+ transport at low temperatures [58]; (2) Low desolvation energy barriers of solvation structures to facilitate rapid Na^+ desolvation [24]; (3) *In situ* formation of robust electrode-electrolyte interfaces with high Na^+ transference numbers to facilitate rapid interfacial Na^+ migration [59]; (4) Cost-effectiveness and environmental sustainability for scalable deployment [60]. Currently, academia primarily evaluates the low-temperature adaptability of electrolyte systems from two dimensions: half cell and full cell systems. Half cell studies focus on low-temperature performance optimization of single electrode materials, having achieved significant breakthroughs in electrolyte compatibility with various electrode materials. In contrast, full cell systems require simultaneous coordination of divergent electrolyte requirements from cathode and anode materials, facing more complex challenges. This review will systematically summarize recent advancements in low-temperature electrolyte research from both half cell and full cell perspectives.

3.1. Half cell perspectives

3.1.1. Anode materials

Hard carbon (HC) is currently regarded as a promising anode material candidate for commercial sodium-ion batteries [61]. Therefore, it is significantly essential to boost the low-temperature performance of HC for promoting the application of SIBs in energy storage under extremely low-temperature conditions. Weakly solvating electrolyte (WSE) with anion-rich solvation structure has attracted extensive attention for rechargeable batteries [62]. The unique solvation structure shows a low desolvation energy barrier, while facilitates the formation of robust inorganic-rich solid electrolyte interface (SEI) with rapid ion diffusion kinetics [63]. Therefore, WSE shows a huge potential to improve the low-temperature sodium storage performance of electrode materials. For example, Wang's group applied weakly coordinating tetrahydrofuran (THF) as sole solvent to construct the WSE, which effectively enhances the low-temperature sodium performance of HC [64]. The weakly coordinating ability of THF promotes more anion to occupy the inner Na^+ solvation sheath. The unique solvation structure not only minimizes Na^+ desolvation energy, but also promotes the formation of homogeneous SEI with well-distributed NaF and organic component, enabling superior interfacial kinetics even at subzero temperatures. Therefore, the HC anode exhibits exceptional low-temperature fast-charging capability, maintaining 95 % capacity retention with a reversible capacity of 181 mAh/g after 1000 cycles even under harsh conditions (−20 °C, 2 A/g). These demonstrate the remarkable interfacial stability and rapid Na^+ diffusion kinetics. Subsequently, Li's group incorporated 2-methyltetrahydrofuran (2MeTHF) into THF-based electrolytes to further expand the low-temperature operation range of HC anodes (Fig. 3a) [62]. The

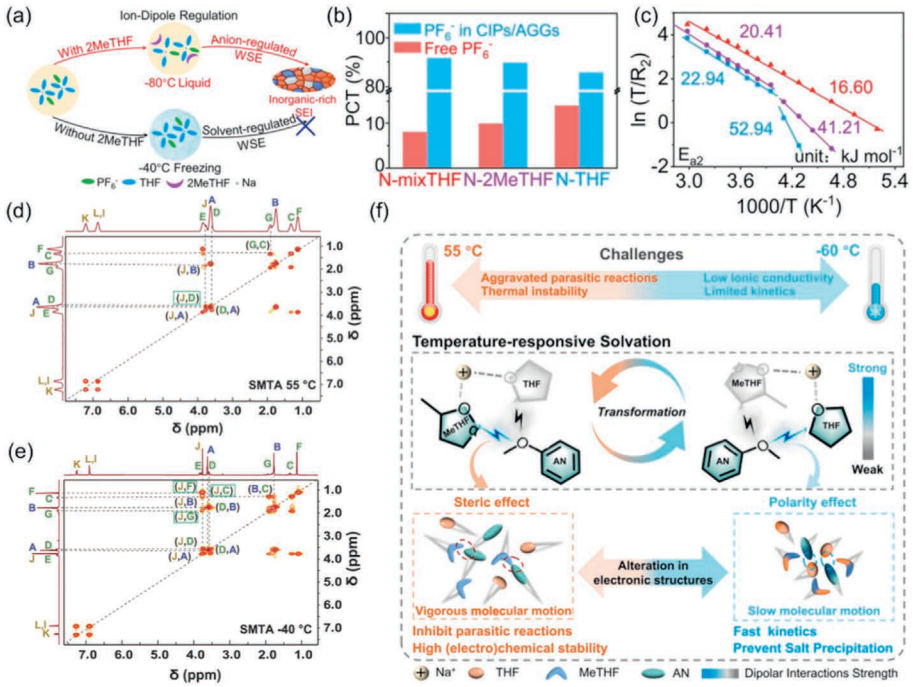


Fig. 3. (a) Mechanism of Na^+-dipole regulation on formation of inorganic-rich SEI. (b) Ratio of different coordinated structures. (c) Na^+ desolvation derived from varying-temperature Nyquist plots. Reprinted with permission [62]. Copyright 2024, Wiley-VCH. ^1H-^1HCOSY nuclear magnetic resonance (NMR) spectra of SMTA electrolyte at (d) 55 °C and (e) −40 °C. (f) Schematic illustration of challenges encountered by wide-temperature electrolytes and temperature-adaptive transformation of solvation structures in SMTA electrolyte. Reprinted with permission [66]. Copyright 2024, Springer Nature.

2MeTHF effectively decreases the ion-dipole interaction, which facilitates more anions and fewer solvents occupying the inner Na^+ solvation structure (Fig. 3b). Noticeably, the anion-enhanced solvation structures are well maintained in a wide temperature range, enabling the formation of robust inorganic-rich SEI. In addition, the designed WSE exhibits a low freezing point of −83.3 °C and high Na^+ transference number of 0.54. More importantly, the energy barrier of Na^+ desolvation and Na^+ diffusion through the SEI are significantly decreased with the addition of 2MeTHF, ensuring the fast interfacial kinetics (Fig. 3c). Benefiting from these merits, the HC anode demonstrates a high reversible capacity (243.2 and 205.4 mAh/g even at −40 and −60 °C, respectively) and excellent cycling stability (negligible capacity degradation after 250 cycles at −40 °C). Noticeably, WSE can significantly improve the low-temperature performance of HC anode, but suffer from low ionic conductivity and poor salt solubility. Therefore, it is imperative to develop a WSE with high ionic conductivity and superior salt solubility, which could further enhance the low-temperature performance of SIBs [65].

To achieve the wide-temperature stable operation of SIBs, Lu's group proposed a temperature-adaptive electrolyte by employing an anti-solvent (anisole, AN) to regulate the dipole-dipole interactions in MeTHF/THF-based electrolyte (SMTA) [66]. They disclose significant temperature-dependent evolution of solvation structures in the SMTA electrolyte (Figs. 3d-f). At elevated temperature, a THF-dominated solvation structure is observed due to the increased dipole-dipole interaction between AN and MeTHF. In contrast, a stronger dipole-dipole interaction between AN and THF induces a MeTHF-dominated solvation structure at low temperature. This unique temperature-responsive behavior endows the SMTA electrolyte with dual advantages: (1) Superior high-temperature stability to suppress the parasitic reactions and (2) low freezing point to avoid salt precipitation. These enable a stable operation at a wide temperature range of −60~55 °C, the HC anode delivers a capacity retention of 73.5 % after 250 cycles at 55 °C and 87 % after 700 cycles at −40 °C. These results demonstrate that the SMTA electrolyte is a promising candidate for wide-temperature SIBs.

The entropy effects of electrolytes have attracted extensively attention in recent years. The entropy of electrolyte is closely related to the physicochemical properties, which remarkably influences the low-temperature sodium storage performance [33]. In general, rational modulation of electrolyte entropy can effectively enhance ionic conductivity, accelerate desolvation process, lower freezing points, while facilitate the formation of stable EEIs [67]. For example, You's group developed an entropy-driven solvation in electrolyte with strong-solvation and weak-solvation solvent mixture to achieve improved ionic conductivity, which greatly enhances the electrochemical stability at low temperature (Figs. 4a and b) [68]. The designed electrolyte owns a temperature-adaptive feature, effectively avoiding the salt precipitation (Fig. 4c). In addition, the solvation structure at low temperature is in favor of the extraction of anion, ensuring a fast co-intercalation process in the HC anode. X-ray photoelectron spectroscopy (XPS) reveals that the temperature-adaptive solvation structure tunes the SEI composition toward more ion conductive nature at low temperature (Figs. 4d and e). Therefore, HC anode shows a negligible capacity degradation after 500 cycles at −40 °C. Meanwhile, HC||$Na_{2/3}Ni_{1/4}Cu_{1/12}Mn_{2/3}O_2$ full cells with the designed electrolyte deliver a high capacity retention of 90.6 % after 400 cycles at −40 °C, demonstrating the huge potential for practical application. More importantly, the universality of this electrolyte design strategy is verified by a series of strong-solvation and weak-solvation electrolytes. Similarly, a high-solvation-entropy electrolyte with a high ionic conductivity of 13.87 mS/cm and Na^+ transference number of 0.32 at −40 °C is reported by Wang's group [69]. The high entropy electrolyte promotes the formation of anion-derived, thin, and NaF-rich SEI layer on HC surface with fast interfacial ion transfer. Therefore, the HC anode shows a high capacity retention of 80.6 % after 1400 cycles at −40 °C. As shown in Figs. 4f-h, the undesirable sodium metal plating in HC||$Na_3V_2(PO_4)_3$ full cells

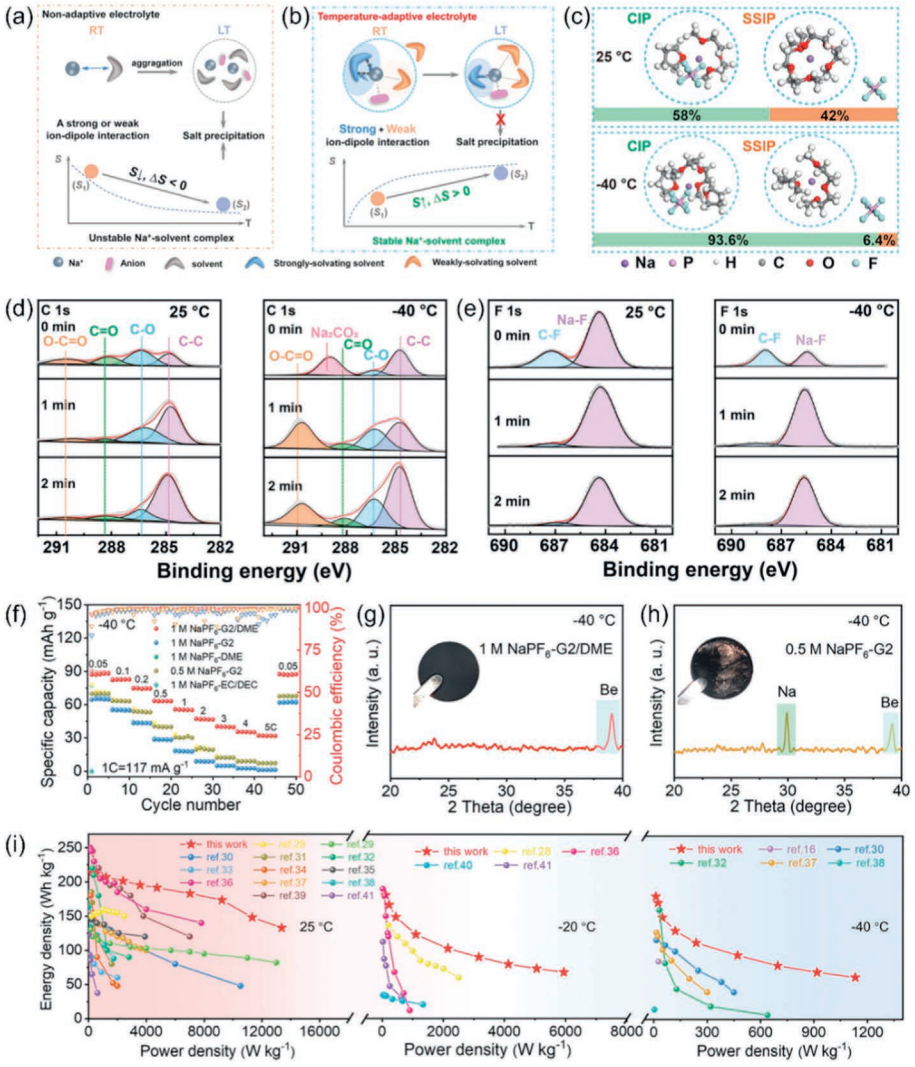


Fig. 4. The solvation structure variations with temperature driven by entropy change: (a) Non-adaptive electrolyte; (b) temperature-adaptive electrolyte. (c) Representative solvation structures for the optimized electrolyte at 25 and −40 °C. (d) C 1s and (e) F 1s XPS spectra of the cycled HC electrodes at 25 °C and −40 °C. Reprinted with permission [68]. Copyright 2023, Wiley-VCH. (f) Rate performance of HC||$Na_3V_2(PO_4)_3$ full batteries at −40 °C. X-ray diffraction patterns and digital photographs (insets) of HC anodes with (g) 1 mol/L $NaPF_6$-G2/DME and (h) 0.5 mol/L $NaPF_6$-G2 electrolytes. (i) Ragone plots of full battery with previously reported SIBs at 25, −20, −40 °C (all based on the total mass of active materials on anode and cathode). Reprinted with permission [69]. Copyright 2024, Wiley-VCH.

at −40 °C is avoided by using high-solvation-entropy electrolyte, which effectively improves the fast-charging performance. More importantly, the HC||$Na_3V_2(PO_4)_3$ full cells show a record-high power density of 1132.31 W/kg at −40 °C (Fig. 4i). Recently, Chen's group designed a temperature-adaptive solvation structure by introducing ultraweak solvent (1,3-dioxolane, DOL) into the diglyme (G2)-based electrolyte, which balances the high ionic conductivity and low desolvation energy barrier [70]. The dipole-dipole interaction between DOL and G2 induces an anion-reinforced solvation structure at low temperature, which effectively reduces the desolvation energy barriers. Furthermore, the unique solvation structure facilitates the formation of robust inorganic-rich SEI, ensuring fast Na^+ transport at low temperature. Even at −40 °C, the Na||HC half cells achieve high reversible capacity (220.8 mAh/g) and superior cycling stability (capacity retention of 91.9% after 900 cycles). However, the existence of multiple solvents/salts not only increases the complexity of electrolyte preparation, but also possibly compromises the intrinsic advantages of individual components while amplifying their inherent limitations. Therefore, the development of high-entropy electrolytes based on simple components holds significant scientific and practical importance.

Apart from solvent optimization, introducing electrolyte additives is also an effective strategy to boost sodium storage performance [71]. Electrolyte additives represent a simple, effective, and economical strategy for enhancing battery performance. Electrolyte additives can modify the Na^+ solvation structure and simultaneously facilitate the construction of uniform and stable EEIs, which effectively accelerate interfacial kinetics [72]. For instance, Li and co-workers proposed an electrolyte reconfiguration strategy based on the hard and soft acid and base theory by introducing methyltriphenylphosphonium bromide (MTPPB) additive [73]. MTPPB can realize a spontaneous cross-coordination solvation structure with $NaPF_6$ through the $MTPP^+$-PF_6^- and Na^+-Br^- interaction, which significantly reduces the coordination number of solvent with accelerated desolvation kinetics. Meanwhile, the unique chemical π-π bridging of $MTPP^+$-HC ensures the preferential decomposition of PF_6^- for a NaF-rich low-impedance supramolecular SEI layer. As a result, the HC anode with MTPPB-containing electrolyte shows an obvious improved reversible capacity, initial Coulombic efficiency, rate performance and cycling stability at −20 °C.

Alloy anodes with high reversible capacity are also applied in SIBs [74]. Wang's group incorporated MeTHF into dimethoxyethane

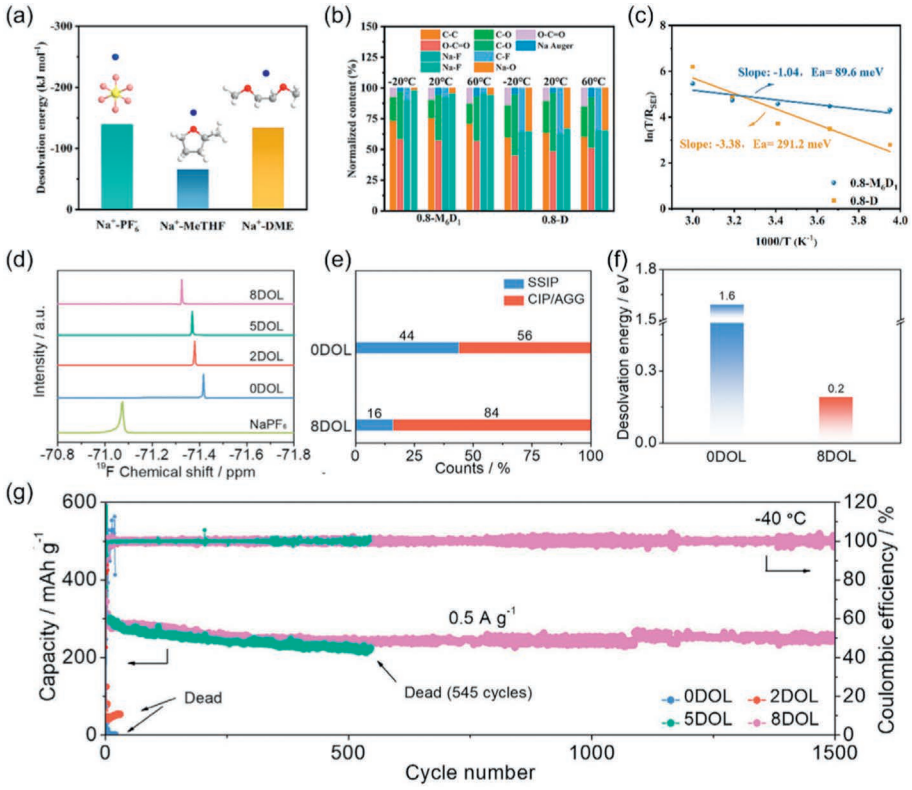


Fig. 5. (a) Desolvation energy of Na^+ with PF_6^-, MeTHF and DME. (b) Arrhenius plot of R_{SEI} with derived E_a for Bi in two electrolytes. (c) Relative content of different species in SEI layers at three temperatures. Reprinted with permission [75]. Copyright 2023, Elsevier. (d) ^{19}F NMR of different electrolytes. (e) The ratio of SSIP and CIP/AGG, and (f) desolvation energy of different electrolytes. (g) Cycling performance of Na||Sn at −40 °C. Reprinted with permission [76]. Copyright 2025, Wiley-VCH.

(DME)-based electrolyte to obtain a temperature-independent anion-reinforced solvation structure (Fig. 5a) [75]. The anion-reinforced solvation structure not only reduces the desolvation energy of Na^+ but also facilitates the formation of stable NaF-rich SEI layer with low Na^+ diffusion barriers (Fig. 5b). Compared with DME-based electrolyte, the energy barrier of Na^+ across the SEI layer in MeTHF/DME-based electrolyte is reduced from 291.2 meV to 89.6 meV (Fig. 5c). Therefore, the Bi||Na half cell achieves stable operation in a wide temperature range from −40 °C to 80 °C, exhibiting a high capacity retention of 96.34 % after 300 cycles at −20 °C. In addition, the potential of the designed electrolyte for practical wide-temperature SIBs is demonstrated by HC||$Na_3V_2(PO_4)_3$ full cell. Similarly, Yang and co-workers introduced DOL as co-solvent into G2-based electrolyte to boost the low-temperature sodium storage performance of Sn anode [76]. DOL effectively regulates the solvation structure, enabling the reduced desolvation energy and constructing a robust SEI (Figs. 5d-f). As shown in Fig. 5g, the commercial Sn microparticles anode shows a superior cycling stability even at −40 °C, maintaining a high capacity retention of 79.3 % after 1500 cycles.

3.1.2. Cathode materials

Cathode material as a key component of SIBs is closely related to the electrochemical performance. Therefore, various electrolyte design strategies are employed to improve the low temperature sodium storage of cathode materials. For example, Wang's group developed a weakly solvating ester-based electrolyte to accelerate the charge transfer kinetics for high-voltage $Na_3V_2(PO_4)_2F_3$ cathode [77]. As shown in Fig. 6a, solvent-separated ion pair with weakly-bonded Na^+/solvent structure is formed in the designed electrolyte. The unique solvation structure facilitates the formation of a dense and uniform cathode-electrolyte interface (CEI) on the surface of $Na_3V_2(PO_4)_2F_3$ cathode, which effectively boosts the interfacial kinetics (Figs. 6b and c). In addition, the structural stability of $Na_3V_2(PO_4)_2F_3$ cathode materials is significantly improved by using the designed weakly solvating electrolyte. Therefore, both of Na||$Na_3V_2(PO_4)_2F_3$ half cells and HC||$Na_3V_2(PO_4)_2F_3$ full cells deliver superior rate performance and cycling stability at −25 °C. Similarly, they reported a weakly solvated ether-based electrolyte to unlock the application of $Na_3V_2(PO_4)_2F_3$ cathode materials at extremely low temperature conditions. Subsequently, You's group designed a high-voltage THF-based electrolyte for low-temperature SIBs [78]. The strategic incorporation of propylene carbonate (PC) and ethoxy(pentafluoro)cyclotriphosphazene (PFPN) synergistically improve the anti-oxidation stability and avoid electrolyte crystallization at low temperature (Fig. 6d). This optimized formulation concurrently facilitates the formation of thin, robust, and inorganic-dominated CEI on $Na_{2/3}Mn_{2/3}Ni_{1/3}O_2$ surface, ensuring the superior electrochemical performance (Figs. 6e and f). As expected, the Na||$Na_{2/3}Mn_{2/3}Ni_{1/3}O_2$ cell delivers 89.3 % of its room-temperature capacity with a high capacity retention of 94.1 % after 100 cycles at −40 °C, significantly higher than the pure THF-based electrolyte (Figs. 6g-i).

Carboxylate esters have emerged as promising electrolyte solvents for low-temperature SIBs due to their advantageous low melting point and viscosity [79]. Recently, Wu's group developed a methyl propionate (MP)-based electrolyte by incorporating fluoroethylene carbonate (FEC) as film-forming co-solvent, which remarkably enhances the low-temperature performance of SIBs [80]. This engineered electrolyte demonstrates dual functionality: (1) Endows superior ionic conductivity and ultra-low melting point; (2) Promotes the formation of robust CEI on high-voltage $Na_3V_2(PO_4)_2O_2F$ cathode surfaces. The robust CEI layer plays a pivotal role in optimizing Na^+ transport kinetics while ensuring interfacial stability. These synergistic effects enable un-

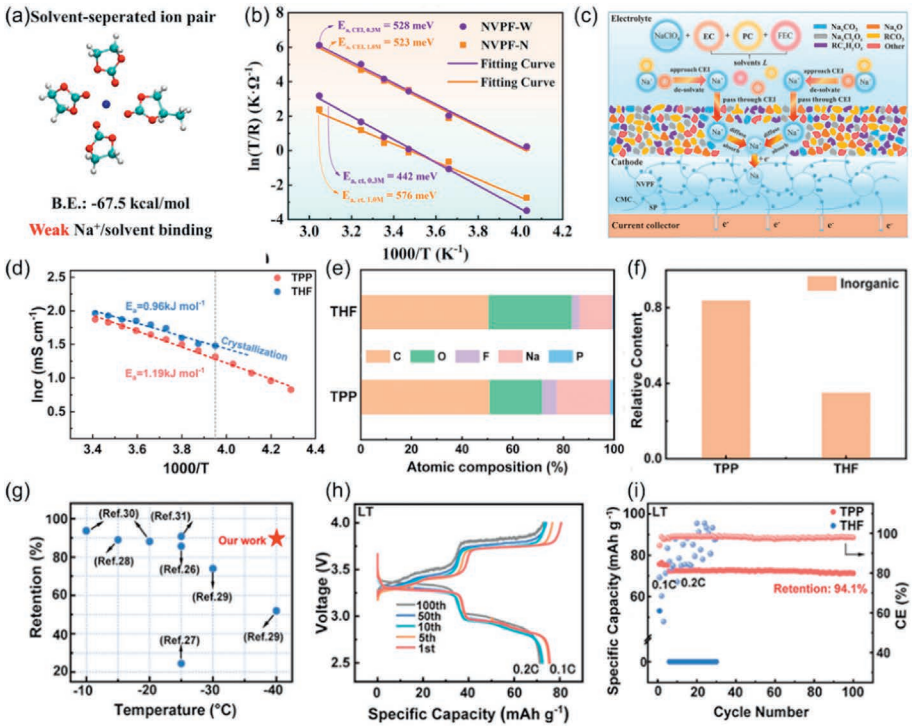


Fig. 6. (a) Most probable solvation structure together with their binding energy values. (b) Arrhenius plots for charge transfer resistance (R_{ct}) and the resistance corresponding to Na^+ transport through the compact CEI (R_{CEI}) of the $Na_3V_2(PO_4)_2F_3$ cathodes in different electrolytes. (c) Schematic illustration of $Na_3V_2(PO_4)_2F_3$/interface/electrolyte system in the weakly-solvating electrolyte. Reprinted with permission [77]. Copyright 2021, Elsevier. (d) Ionic conductivity of electrolyte at different temperatures. (e) Relative content of elements. (f) Relative content of inorganic products calculated from the XPS data. (g) Capacity retention of cells employing a variety of electrolytes compared to the capacity at room temperature as a function of temperature. (h) Charge/discharge curves for different cycles at −40 °C. (i) Cycling performance at −40 °C. Reprinted with permission [78]. Copyright 2023, American Chemical Society.

precedented electrochemical performance, achieving stable operation of Na||$Na_3V_2(PO_4)_2O_2F$ cells at extreme low-temperature conditions (−40 °C), maintaining 96 % capacity retention after 100 cycles. Subsequently, Pang's group employed ethyl propionate (EP) to realize all-climate SIBs operating across a wide temperature range (Fig. 7a) [81]. The introduction of EP into conventional ester-based electrolytes significantly decreases the glass transition temperature and enhances the ion conductivity (Figs. 7b and c). Concurrently, sodium difluoro(oxalato)borate (NaDFOB) and succinonitrile (SN) were employed as synergistic film-forming additives, effectively promoting the formation of uniform inorganic-rich EEI (Fig. 7d). As shown in Figs. 7e and f, the Na||$Na_3V_2(PO_4)_3$ half cell exhibits exceptional cycling stability and remarkable rate capability across an extensive temperature at a wide temperature range from −45 °C to 60 °C.

Low-concentration electrolytes have attracted significant attention due to their advantages such as low cost and low viscosity, but their relatively poor low-temperature performance hinders their practical applications [82]. Xie's group employed 2,2,2-trifluoroethyl acetate (ETFA) as multifunctional additive into a dilute electrolyte (0.5 mol/L) to address low-temperature challenges in SIBs [83]. The ETFA-containing electrolyte shows a high ionic conductivity and low viscosity. In addition, the ETFA effectively weakens the interaction between Na^+ and solvents due to the strong electron-withdrawing effect of -CF_3 group, enabling a fast desolvation process. Concurrently, ETFA decomposition contributes to a robust F-rich EEI with fast Na^+ transport kinetics. As a result, the FeNi co-doped Mn-based Prussian blue cathode exhibits a high capacity retention of 92.1 % after 1120 cycles at −20 °C. Similarly, Qiao *et al.* developed a low concentration electrolyte to boost the wide-temperature performance, which owns the advantages of low cost, rapid ion diffusion and superior wetting properties [84]. Compared with the conventional concentration electrolyte, the Na||$FePO_4$ cell with low concentration electrolyte shows a better electrochemical performance at the wide temperature range (−20∼55 °C).

In general, high desolvation energy barrier is the critical factor that limits the low-temperature performance of sodium-ion batteries. Li's group employed high electron affinity of the trifluoroacetate anion (TFA^-) to regulate the solvation chemistry of 1.0 mol/L $NaPF_6$-G2 electrolyte, achieving an anion-reinforced solvation structure at conventional concentrations to significantly reduce the desolvation energy (Figs. 8a and b) [24]. As confirmed by ^{23}Na NMR, Raman spectra and theoretical calculations, the TFA^- preferentially occupies the inner solvation sheath of Na^+ (Fig. 8c). Compared with the 1.0 mol/L $NaPF_6$-G2 electrolyte, the strongly coordinating TFA^- enables more PF_6^- anions and fewer G2 molecules to occupy the inner solvation structure, which accelerates the interfacial desolvation process with decreased desolvation energies (Figs. 8d and e). Even at −40 °C, the Na||$Na_3V_2(PO_4)_3$ cell delivers 60.2 % of its room-temperature capacity with a high capacity retention of 99.2 % after 100 cycles. Notably, variable-temperature molecular dynamics simulations and Raman spectra reveal the temperature-dependent solvation structure evolution, where the coordination number of PF_6^- anions significantly increases with decreasing temperature (Figs. 8f and g). Subsequently, they integrated THF into G2-based electrolyte to construct the anion-rich solvation structure. This tailored solvation structure significantly reduces desolvation energy while promotes the formation of robust NaF-rich electrode-electrolyte interface, which concurrently enables homogeneous sodium deposition and enhances interfacial ion-transport kinetics. In addition, they develop a carbon nanotubes-modified P2-$Na_{0.67}Mn_{0.67}Ni_{0.33}O_2$ (NMNO-CNTs) cathode, effectively addressing electron transport limitations in con-

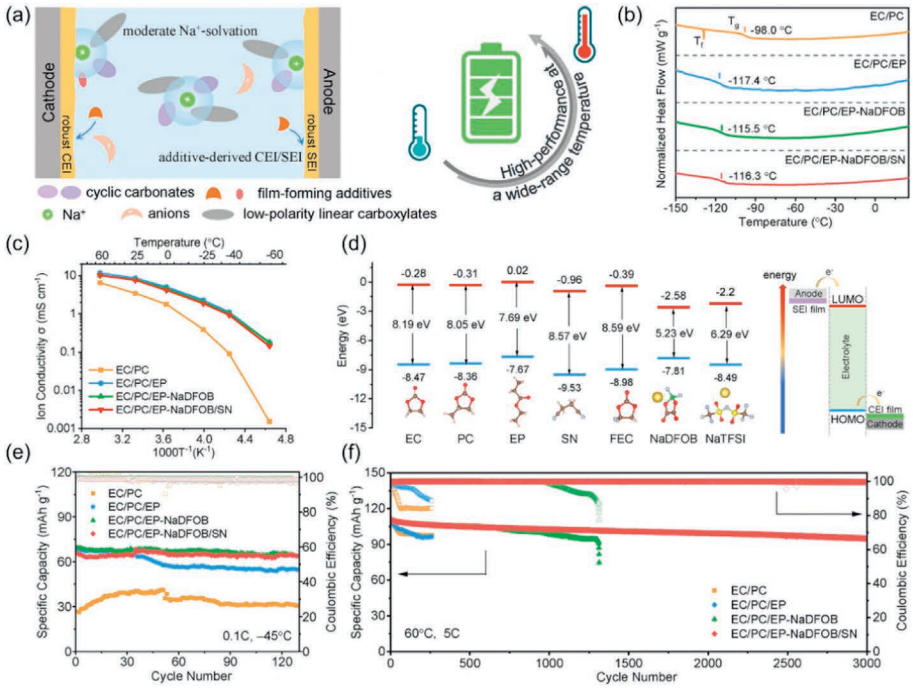


Fig. 7. (a) Illustration of electrolyte design with fast ion transport and excellent film-forming property for all-climate SIBs. (b) Differential scanning calorimetry (DSC) curves of the various electrolytes. (c) Ionic conductivity at different temperatures. (d) Calculated lowest unoccupied molecular orbital and highest occupied molecular orbital energy levels of solvent molecules, sodium salts, additives. (e) Capacity retention of Na||$Na_3V_2(PO_4)_3$ cells using varied electrolytes at −45 °C. (f) Capacity retention of Na||$Na_3V_2(PO_4)_3$ cells using varied electrolytes at 60 °C. Reprinted with permission [81]. Copyright 2024, Wiley-VCH.

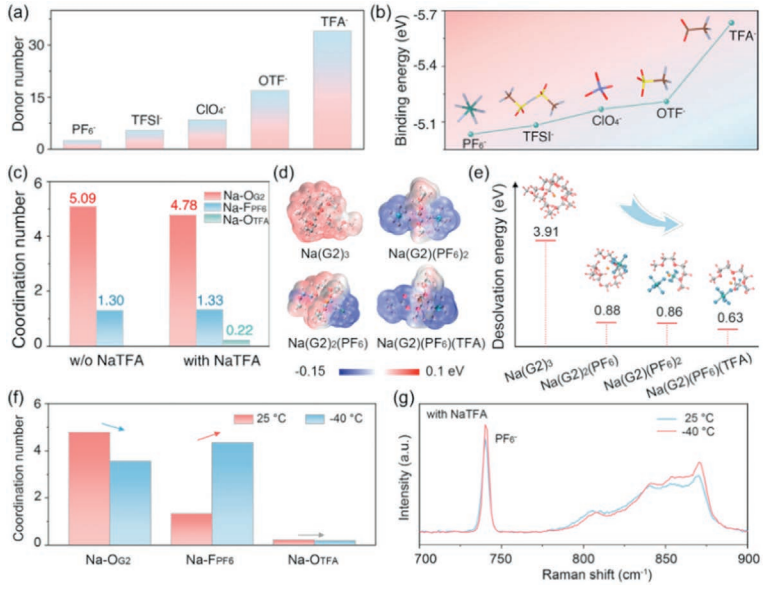


Fig. 8. (a) Donor number of commonly used anions. (b) Binding energy of Na^+ with anions. (c) Coordination number from MD simulations. (d) Electrostatic potential density distribution, and (e) desolvation energy of representative solvation configurations. (f) Coordination number of solvents and anions and (g) Raman spectra at 25 °C and −40 °C. Reprinted with permission [24]. Copyright 2024, National Academy of Sciences.

ventional layered oxide cathodes [85]. The synergistic effects unlock the charge transfer limitation of SIBs at low temperatures, realizing a superior cycling stability of both half cells and full cells even at −40 °C. More importantly, The HC||$Na_{0.67}Mn_{0.67}Ni_{0.33}O_2$ full cell delivers a high energy density of 237.6 Wh/kg at −40 °C.

The origin of voltage oscillation of SIBs at low temperatures is investigated by Chao's group [86]. Combining the theoretical calculations and *in-/ex-situ* characterization techniques, they demonstrated that voltage oscillation stems from the local phase transition of $Na_3V_2(PO_4)_3$ cathode. To address this challenge, the team designed a G2-based electrolyte to unlock desolvation kinetic limitations and accelerate interfacial ion transport at −40 °C. This optimized electrolyte effectively suppresses local phase transition in $Na_3V_2(PO_4)_3$, eliminating voltage oscillations and enabling remarkable low-temperature performance. The $Na_3V_2(PO_4)_3$ cathode achieves 75.3 % capacity retention at −40 °C. Notably, the sodium titanates||$Na_3V_2(PO_4)_3$ full cell further demonstrates exceptional cycling stability under low temperature, underscoring the viability of this strategy for practical low-temperature SIBs applications.

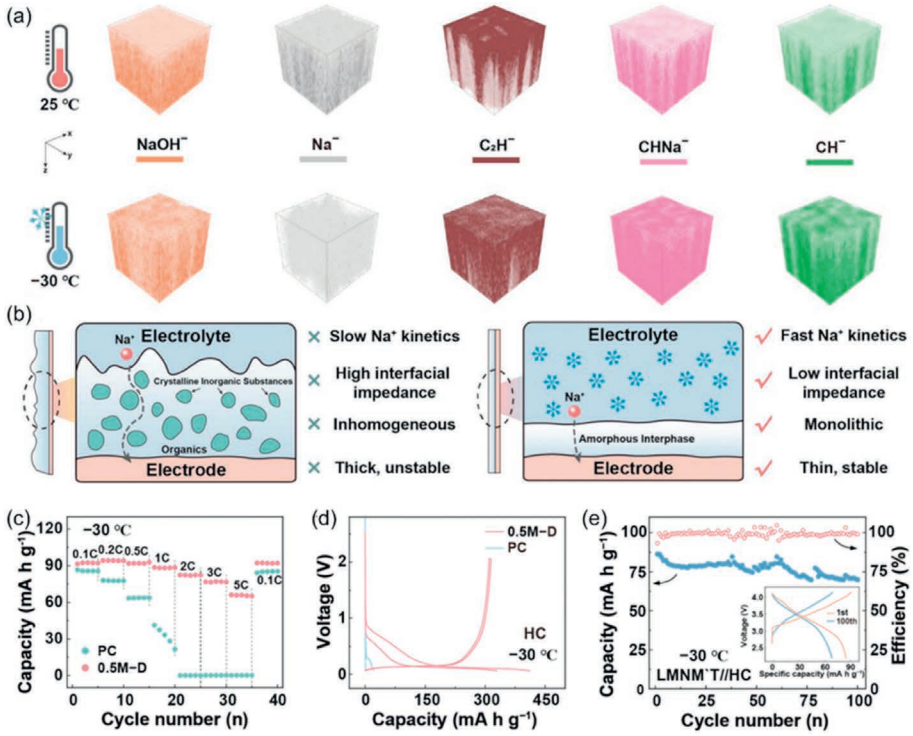


Fig. 9. (a) 3D reconstruction images of $NaOH^-$, Na^-, C_2H^-, $CHNa^-$ and CH^-. (b) Schematic illustration of EEI at different temperatures. (c) Rate performance of half cells at −30 °C. (d) First two charge/discharge curves of HC half cells at −30 °C. (e) Cycling performance and charge/discharge curves of HC||$Na_{0.7}Li_{0.03}Mg_{0.03}Ni_{0.27}Mn_{0.6}Ti_{0.07}O_2$ full cells at −30 °C. Reprinted with permission [59]. Copyright 2024, Wiley-VCH.

3.2. Full cell perspectives

The simultaneous optimization of the electrochemical performance of both cathode and anode materials at low temperatures represents a critical breakthrough in constructing high-performance sodium-ion full batteries and accelerating their commercialization. Lu's group proposed a low-concentration electrolyte (0.5 mol/L $NaPF_6$ in G2, 0.5M-D) that facilitates the formation of thin, amorphous, homogeneous and organic-rich CEI at low temperature (Fig. 9a) [59]. As shown in Fig. 9b, the as-formed CEI effectively improves the interfacial Na^+ dynamics due to the faster Na^+ migration through organic components than inorganic components. In addition, the side reaction between electrode materials and electrolyte during the charge/discharge process is eliminated, enabling a superior structural stability of electrode materials. Compared with the conventional electrolyte, the low temperature sodium storage performances of $Na_{0.7}Li_{0.03}Mg_{0.03}Ni_{0.27}Mn_{0.6}Ti_{0.07}O_2$ cathode and HC anode are simultaneously improved in the designed electrolyte (Figs. 9c and d). More importantly, the full cells deliver a high capacity retention of 83.2 % after 100 cycles at −30 °C (Fig. 9e).

Subsequently, Wu's group introduced tris(trimethylsilyl) phosphite (TMSPi) and FEC as additives into PC-based electrolyte to realize a ultrawide-temperature SIBs [87]. As shown in Fig. 10a, TMSPi exhibits a dual role on acting as a sacrificial agent for film formation while synergizing with FEC to generate reactive intermediates *via* interfacial decomposition. During FEC's defluorination hydrolysis producing HF, it simultaneously exhibits superior HF scavenging capability. In addition, the oxidative decomposition of TMSPi favors the stable CEI on the surface of the cathode, while FEC facilitates the formation of robust SEI on HC anode. The robust CEI/SEI features improved ion transport capability and excellent structural/thermal stability, ensuring a superior electrochemical performance of both cathode and anode at a wide temperature range (Fig. 10b). As shown in Figs. 10c-g, HC||$Na_3V_2(PO_4)_2O_2F$ full cells show excellent adaptability over a wide temperature range from −25 °C to 50 °C, maintaining a high capacity retention of 94 % after 500 cycles at −25 °C and 93 % after 1000 cycles at 50 °C. Noticeably, Nan's group applied trimethylsilyl methanesulfonate (TMSS) as trifunctional additive to boost the low-temperature sodium storage of carbonate ester-based electrolyte [88]. The solvation structure is regulated by TMSS, resulting in a significant decrease in desolvation energy from 64.11 kJ/mol to 46.84 kJ/mol. Meanwhile, the HF and water are effectively removed after incorporation of TMSS, ensuring a superior structural stability of electrode materials. The introduction of TMMS induces the formation of robust sulfur-rich CEI and silicon-rich SEI films, which effectively avoids the interfacial side reactions. Therefore, the assembled HC||$NaNi_{0.33}Fe_{0.33}Mn_{0.33}O_2$ pouch full cell shows a superior cycling stability at high cut-off voltage of 4.0 V and wide temperature range (−30–60 °C). They also proposed a "hard-soft synergy" strategy to design functional multi-component electrolytes for wide-temperature SIBs [89]. Coupling "hard"-sodium difluorophosphate (NaDFP) with "soft"-tris(trimethylsilyl)borate (TMSB) to enable an anion collaborative solvation structure, which facilitates the formation of tough and multi-component EEI for improved cycling stability. In addition, the designed electrolyte owns a low desolvation energy barriers and viscosity, ensuring a superior low-temperature performance. Compared with conventional electrolyte, the cycling stability of HC||$NaNi_{0.33}Fe_{0.33}Mn_{0.33}O_2$ full cell with the designed electrolyte is significantly improved, maintaining a high capacity retention of 95 % after 350 cycles at −10 °C.

Sodium salts, as essential components of electrolytes, play a pivotal role in determining both the physicochemical properties and manufacturing costs of the electrolytes [90]. In addition, the types of salt are closely related to the solvation structure and the EEIs. Rational optimization of sodium salt species enables effective tailoring of the solvation structure, which consequently reduces

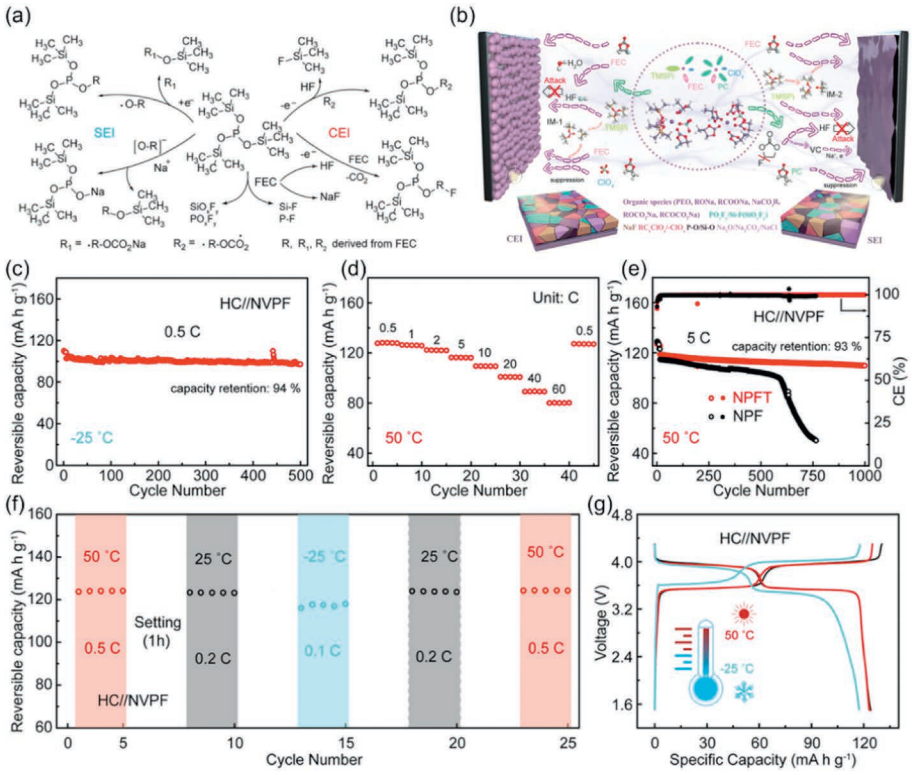


Fig. 10. (a) Diagram of synergistic regulatory mechanisms driven by distinct intermediates for interfacial modification and HF consumption with the role played by TMSPi and FEC. (b) Schematic diagram of the synergistic film-forming mechanisms induced by phosphorus/silicon-intermediates and the self-purification process in designed electrolyte. (c) Cycling performances at −25 °C. (d) Rate capabilities and (e) comparison of cycling performances at 50 °C. (f) Continuous temperature test simulating widespread all-weather conditions and (g) corresponding charge/discharge curves. Reprinted with permission [87]. Copyright 2024, American Chemical Society.

the desolvation energy barrier of Na^+ and enhances interfacial ion transport kinetics. This strategic approach leads to remarkable improvement in the low-temperature electrochemical performance of SIBs [91]. Recently, Cao and coworkers achieved breakthrough cycle stability and low-temperature performance in SIBs through innovative application of NaDFOB-based ether electrolytes [92]. As shown in Fig. 11a, NaDFOB is prepared *via* a facile and scalable liquid precipitation technique, demonstrating the huge potential for practical application. As shown in Figs. 11b-d, the NaDFOB promotes the formation of dense, robust EEI on electrode surfaces, significantly enhancing the interfacial stability. This enables Ah-level HC||$Na_4Fe_3(PO_4)_2P_2O_7$ pouch cell with NaDFOB-based ether electrolyte to maintain stable operation at a wide temperature range from −40 °C to 60 °C, showing an excellent cycling stability at −20 and 60 °C (Figs. 11e and f). Similarly, Ma's group employed electron-attracting $DFOB^-$ anions to establish an anion-reinforced solvation architecture, effectively weakening Na^+-solvent interactions through synergistic coordination [93]. The unique solvation structure enables accelerated desolvation kinetics, significantly enhancing the rate capability of SIBs. In addition, the electrolyte formulation facilitates the concurrent formation of dense, stable and inorganic-rich EEI on cathode and anode surface, which effectively inhibits the side reaction and irreversible phase transition. Therefore, the HC||$Na_4Fe_3(PO_4)_2P_2O_7$ pouch cell with the designed electrolyte exhibits excellent cycling stability, achieving capacity retention rate of 98.3 % and average CE of >99.8 % after 500 cycles at −20 °C.

4. Summary and outlook

SIBs are regarded as promising candidates for large-scale energy storage systems in extreme low-temperature environments due to their abundant sodium resource reserves, low manufacturing costs, and potential advantages in low-temperature adaptability. As a core component of SIBs, electrolytes play a key role on Na^+ transfer kinetics, significantly influencing the low-temperature performance. This review systematically summarizes recent advancements in organic liquid electrolytes for low-temperature SIBs. We firstly analysis the failure mechanisms of SIBs under low-temperature conditions from the perspective of charge transfer kinetics. Subsequently, comprehensive electrolytes optimization strategies for low-temperature SIBs are discussed from both half cell and full cell dimensions. In general, the key physicochemical parameters of electrolyte (ionic conductivity, viscosity, freezing point, *etc.*), solvation structures and electrode-electrolyte interfacial chemistry can be regulated by electrolyte component optimization (including solvent regulation, sodium salt selection, and additive incorporation) and salt concentration engineering (Fig. 12). The synergistical effects significantly enhance Na^+ transfer kinetics under low-temperature operation, leading to breakthroughs in critical performance metrics such as reversible capacity, rate performance, cycling stability, and Coulombic efficiency. To visually demonstrate the performance enhancement achieved by electrolyte engineering, the electrochemical performance parameters of representative low-temperature sodium-ion battery electrolyte systems are summarized in Table 1.

To promote the development of low-temperature electrolyte for SIBs, we suggest that future researchers focus on following directions (Fig. 13): (1) Revealing the structure-function relationship between solvation structures and EEI chemistry, and elucidating the regulatory mechanism of solvation structures on interfacial charge transfer kinetics. (2) Systematically investigating the temperature-responsive characteristics of solvation structures, with emphasis on the evolution mechanisms of solvation structures and desolvation

Table 1
Representative electrolytes and their low-temperature performance in different battery systems.

Battery	Electrolyte (salt-solvent-additive)	Ionic conductivity (mS/cm)	Viscosity (mPa s)	Rate performance (mAh/g, A/g)	Cycle performance (%)/cycles	Operating temperature (°C)	Ref.
HC||Na	1.0 mol/L $NaPF_6$-THF	/	/	175, 2	95/1000	−20	[64]
HC||Na	1.0 mol/L $NaPF_6$-THF/2MeTHF (5:5, v/v)	1.59	/	/	~97/100	−60	[62]
HC||Na	1.0 mol/L $NaPF_6$−MeTHF/THF/AN (17:17:6, v/v/v)	2.4	3.88	/	87.0/700	−40	[66]
HC||Na	1.0 mol/L $NaPF_6$-G2/THF (2:8, v/v)	3.32	~3.35	/	~95.4/500	−40	[68]
HC||Na	1.0 mol/L $NaPF_6$-G2/DME (1:1, v/v)	13.87	/	97, 2.1	99.5/1000	−40	[69]
HC||Na	0.5 mol/L $NaPF_6$-G2/DOL (1:3, v/v)	3.39	~2.98	/	97.25/200	−50	[70]
HC||Na	0.6 mol/L $NaPF_6$-G2 + 0.25 wt% MTPPB	/	~3.65	112.3, 2.0 C	~99/500	−20	[73]
Bi||Na	0.8 mol/L $NaPF_6$−MeTHF/DME (6:1, v/v)	1.78	/	/	96.34/300	−20	[75]
Sn||Na	1.0 mol/L $NaPF_6$-G2/DOL (2:8, v/v)	2.38	400	~80, 2	79.3/1500	−40	[76]
Na||$Na_3V_2(PO_4)_2F_3$	0.3 mol/L $NaClO_4$-EC/PC (1:1, v/v) + 5% FEC	1.80~2.34	/	101.6, 1.0 C	93.4/1000	−25	[77]
Na||$Na_{2/3}Mn_{2/3}Ni_{1/3}O_2$	0.8 mol/L $NaPF_6$-THF/PC/PFPN	2.3	6.3	/	94.1/100	−40	[78]
Na||$Na_3V_2(PO_4)_2O_2F$	2.0 mol/L $NaPF_6$−MP/FEC (9:1, v/v)	/	/	~38, 0.5 C	96/100	−40	[80]
Na||$Na_3V_2(PO_4)_3$	EC/PC/EP-NaDFOB/SN	~1.35	17.44	/	~95/130	−45	[81]
Na||FeNi-MnHCF	0.5 mol/L $NaPF_6$-PC/EMC (1:1, v/v) + 4 wt% FEC + 1 wt% ETFA	47.8	~7.98	62.8, 10.0 C	83.0/1190	−20	[83]
Na||$FePO_4$	0.3 mol/L $NaPF_6$-PC/FEC/TTE (3:3:4, v/v/v)	2.84	6.72	/	~98/300	−20	[84]
Na||$Na_3V_2(PO_4)_3$	1.0 mol/L $NaPF_6$ + 0.1 mol/L NaTFA-G2	0.27	/	~48, 0.1	99.2/100	−40	[24]
Na||P2-$Na_{0.67}Mn_{0.67}Ni_{0.33}O_2$	1.0 mol/L $NaPF_6$-G2 + 5 vol% THF	0.678	/	89.6, 0.8	92.7/3600	−40	[85]
Sodium titanates||$Na_3V_2(PO_4)_3$	1.0 mol/L $NaPF_6$-G2	/	~18.5	/	99/500	−40	[86]
HC||$Na_{0.7}Li_{0.03}Mg_{0.03}Ni_{0.27}Mn_{0.6}Ti_{0.07}O_2$	0.5 mol/L $NaPF_6$-G2	1.7	/	/	83.2/100	−30	[59]
HC||$Na_3V_2(PO_4)_2O_2F$	1.0 mol/L $NaClO_4$-PC + 10 vol% FEC + 1 vol% TMSPi	/	/	/	94/500	−25	[87]
HC||$NaNi_{0.33}Fe_{0.33}Mn_{0.33}O_2$	1.0 mol/L $NaPF_6$-EC/EMC (3:7 in wt%) + 3 wt%TMSS	~4.1	~10.5	793 mAh, 0.5 C	/	−30	[88]
HC||$NaNi_{0.33}Fe_{0.33}Mn_{0.33}O_2$	0.8 mol/L $NaPF_6$-EC/EMC (3:7, v/v) + 1% NaDFP + 1.5% TMSB	~3.5	~4.5	~620 mAh, 1.0 C	95/350	−10	[89]
HC||$Na_4Fe_3(PO_4)_2P_2O_7$	1.0 mol/L NaDFOB-G2	~2.35	/	/	~80/100	−20	[92]
HC||$Na_4Fe_3(PO_4)_2P_2O_7$	1.0 mol/L $NaBF_4$-G2 + 0.15 mol/L LiDFOB	~0.41	/	~55, 3.0 C	98.3/500	−20	[93]

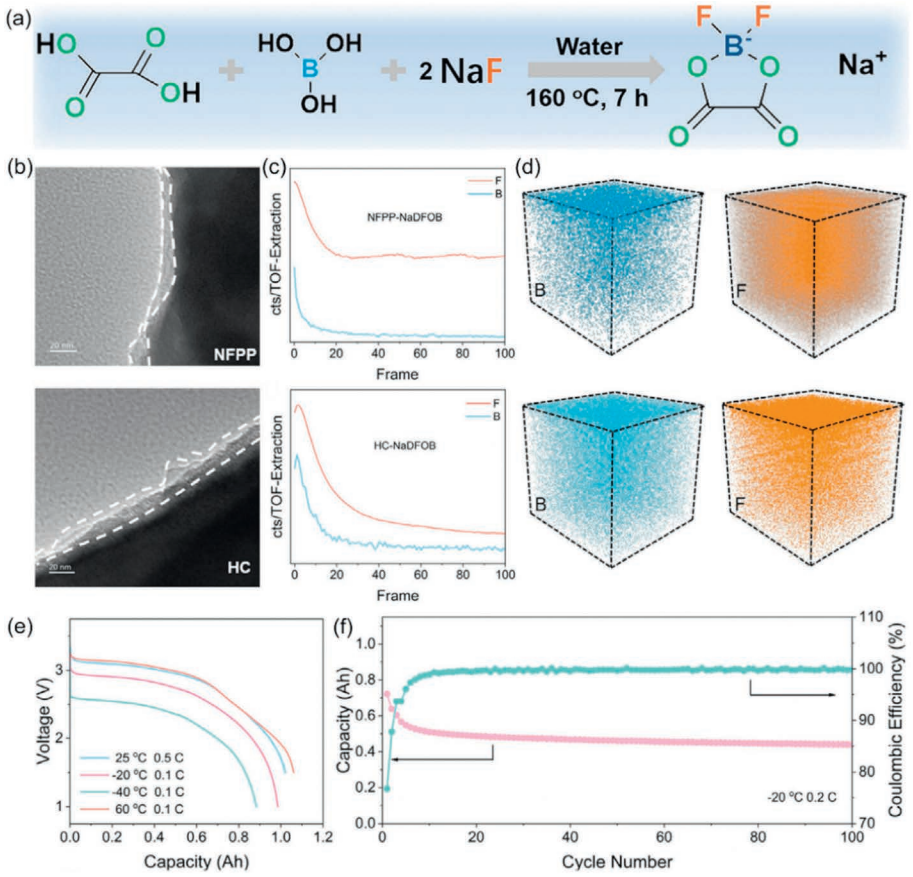


Fig. 11. (a) Schematic illustration of the synthesis of NaDFOB from H_3BO_3, $H_2C_2O_4$, and NaF. (b) TEM images of $Na_4Fe_3(PO_4)_2P_2O_7$ and HC electrodes after cycling. (c) Depth distribution of B^{3+} and F^- ion fragment contents and (d) distribution of elements on $Na_4Fe_3(PO_4)_2P_2O_7$ and HC electrodes analyzed by TOF-SIMS. (e) Discharge curves of HC||$Na_4Fe_3(PO_4)_2P_2O_7$ pouch cell at −20, −40, and 60 °C. (f) Cycling performance of HC|| $Na_4Fe_3(PO_4)_2P_2O_7$ pouch at −20 °C. Reprinted with permission [92]. Copyright 2024, Wiley-VCH.

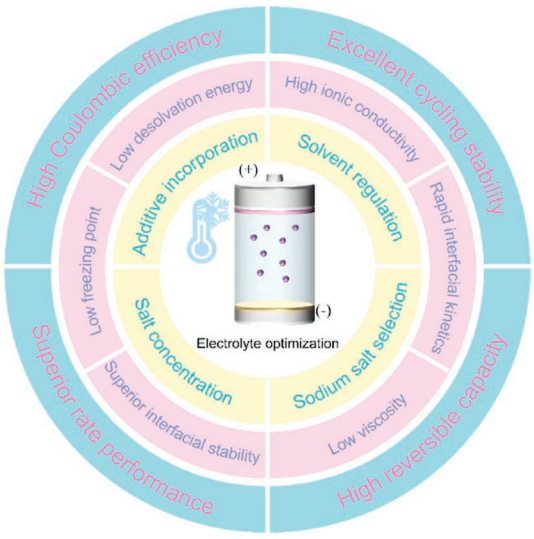


Fig. 12. Various liquid electrolyte designs for low-temperature SIBs.



Fig. 13. Development of electrolytes for low-temperature SIBs.

kinetics under low-temperature conditions. (3) Unlocking the limitations of current low-loading electrodes and small-capacity coin cells for low-temperature performance evaluation, instead adopting high-loading electrodes and large-capacity pouch/cylindrical cells to assess the practical application potential of electrolyte design strategies. (4) Establishing a multi-dimensional database for low-temperature electrolytes, encompassing parameters such as solvent types, salt concentrations, and additive, integrating materials genomics and machine learning technologies for precise electrolyte design. (5) Combining *in-situ* advanced characterization techniques with theoretical calculations to uncover the rate-determining steps

in low-temperature sodium-ion batteries, thereby guiding the design of optimized electrolytes.

CRediT authorship contribution statement

Xiaosa Zhang: Writing – review & editing, Writing – original draft, Conceptualization. **Shanghao Zhou:** Writing – original draft. **Xiaomin Chen:** Writing – original draft. **Xu Xu:** Writing – original draft. **Xiaoyan Shi:** Writing – original draft. **Zhiming Zhou:** Writing – original draft. **Yun Wan:** Writing – original draft. **Xinhui Zeng:** Writing – original draft. **Xunzhu Zhou:** Writing – review & editing, Writing – original draft, Project administration, Funding acquisition, Conceptualization. **Xiang Chen:** Writing – review & editing. **Shu-Lei Chou:** Writing – review & editing, Supervision, Project administration, Funding acquisition, Conceptualization. **Lin Li:** Writing – review & editing, Supervision, Project administration, Funding acquisition, Conceptualization.

Declaration of competing interest

The authors declare that they have no known competing financial interests or personal relationships that could have appeared to influence the work reported in this paper.

Acknowledgments

This work was supported by the National Natural Science Foundation of China (Nos. 52202286, 22309002, 52250710680, 52171217), Key Research and Development Program of Zhejiang Province (No. 2023C01232), Natural Science Foundation of Zhejiang Province (No. LY24B030006), Science and Technology Plan Project of Wenzhou Municipality (Nos. ZG2024055, ZG2022032), Anhui Provincial Natural Science Foundation (No. 2308085QB55), Anhui Postdoctoral Scientific Research Program Foundation (No. 2025B1045), Wenzhou Association for Science and Technology Innovation Program (No. NLTS2024–013), Basic Research Project of Wenzhou City (No. G20220016).

References

[1] K.I. van der Wijst, F. Bosello, S. Dasgupta, et al., Nat. Clim. Change 13 (2023) 434–441.
[2] M. Chen, Y. Zhang, G. Xing, et al., Energy Environ. Sci. 14 (2021) 3323–3351.
[3] A. Gupta, A. Manthiram, Adv. Energy Mater. 10 (2020) 2001972.
[4] A. Hu, F. Li, W. Chen, et al., Adv. Energy Mater. 12 (2022) 2202432.
[5] Y. Cho, H.A. Gabbar, Saf. Extreme Environ. 1 (2019) 11–25.
[6] Y. You, H.R. Yao, S. Xin, et al., Adv. Mater. 28 (2016) 7243–7248.
[7] J. Xie, Y.C. Lu, Nat. Commun. 11 (2020) 2499.
[8] G.J. Yang, Z.M. Hao, C. Fang, et al., Chin. Chem. Lett. 36 (2025) 111185.
[9] Z. Fan, X. Zhou, J. Qiu, et al., Angew. Chem. Int. Ed. 62 (2023) e202308888.
[10] C. Wei, Z. Yao, J. Ruan, et al., Chin. Chem. Lett. 35 (2024) 109330.
[11] F. Zhang, B. He, Y. Xin, et al., Tian, Chem. Rev. 124 (2024) 4778–4821.
[12] F. Duffner, N. Kronemeyer, J. Tübke, et al., Nat. Energy 6 (2021) 123–134.
[13] S. Xin, X. Zhang, L. Wang, et al., Sci. China Chem. 67 (2024) 13–42.
[14] R. Usiskin, Y.X. Lu, J. Popovic, et al., Nat. Rev. Mater. 6 (2021) 1020–1035.
[15] H. Chen, K. Chen, J. Yang, et al., J. Am. Chem. Soc. 146 (2024) 15751–15760.
[16] E. Gabriel, C. Ma, K. Graff, et al., eScience 3 (2023) 100139.
[17] S.Y. Chu, S.H. Guo, H.S. Zhou, Chem. Soc. Rev. 50 (2021) 13189–13235.
[18] Q. Zhu, D. Yu, J. Chen, et al., Joule 8 (2024) 482–495.
[19] Y. Gao, Z. Wang, H. Tu, et al., Adv. Funct. Mater. 35 (2024) 2414652.
[20] M. Li, H. Zhuo, Q. Jing, et al., Carbon Energy 6 (2024) e546.
[21] C. Che, F. Wu, Y. Li, et al., Adv. Mater. 36 (2024) 2402291.
[22] K. Chayambuka, G. Mulder, D.L. Danilov, et al., Adv. Energy Mater. 10 (2020) 2001310.
[23] J. Huang, K. Wu, G. Xu, et al., Chem. Soc. Rev. 52 (2023) 4933–4995.
[24] X.Z. Zhou, Y.H. Huang, B. Wen, et al., Proc. Natl. Acad. Sci. U. S. A. 121 (2024) 2316914121.
[25] X.H. Rui, X.H. Zhang, S.T. Xu, et al., Adv. Funct. Mater. 31 (2021) 2009458.
[26] W. Kuang, X. Zhou, Z. Fan, et al., ACS Energy Lett. 9 (2024) 4111–4118.
[27] S.M. Wu, Y.Y. Li, L.T. Chen, et al., Chin. Chem. Lett. 36 (2025) 109796.
[28] Z. Li, Y. Zhang, J. Zhang, et al., Angew. Chem. Int. Ed. 61 (2022) e202116930.
[29] X. Shi, Z. Hao, W. Zhu, et al., Sci. China Mater. 67 (2024) 3622–3628.
[30] Y. Ren, T. Lai, A. Manthiram, ACS Energy Lett. 8 (2023) 2746–2752.
[31] T. Shi, R. Hou, S. Guo, Energy Lab 1 (2023) 230003.
[32] S. Yang, K. Cheng, Z. Cao, J. Mater. Chem. A 12 (2024) 13059.
[33] D. Peng, R. Sun, J. Han, et al., ACS Energy Lett. 9 (2024) 6215–6224.
[34] X. Zhou, X. Chen, W. Kuang, et al., Angew. Chem. Int. Ed. 63 (2024) e202410494.
[35] J. Chen, Z. Yang, X. Xu, et al., Adv. Mater. 36 (2024) 2400169.
[36] Y. Zheng, D. Wang, S. Kaushik, et al., EnergyChem 4 (2022) 100075.
[37] W. Tian, Z. Li, L. Miao, et al., Adv. Mater. 36 (2023) 2308586.
[38] L. Jiang, S. Han, Y.C. Hu, et al., Nat. Energy 9 (2024) 839–848.
[39] Y. Liu, S.W. Lu, Z.C. Wang, et al., Adv. Funct. Mater. 34 (2024) 2312295.
[40] B. Yi, Z. Wei, S. Yao, et al., Mater. Sci. Eng. R Rep. 163 (2025) 100949.
[41] S.H. Zhou, X.M. Chen, X.S. Zhang, et al., Adv. Funct. Mater. 35 (2025) 2418784.
[42] H. Hijazi, P. Desai, S. Mariyappan, Batteries Supercaps 4 (2021) 881–896.
[43] A. Bauer, J. Song, S. Vail, et al., Adv. Energy Mater. 8 (2018) 1702869.
[44] Y. Sun, B. Liu, L. Liu, et al., Adv. Funct. Mater. 32 (2021) 2109568.
[45] F. Meng, H. Zhang, X. Xiong, et al., R. Hu, Small 20 (2023) 2304806.
[46] J. Zhou, Y. Wang, J. Wang, et al., Energy Storage Mater. 50 (2022) 47–54.
[47] Z. Li, Y.X. Yao, S. Sun, et al., Angew. Chem. Int. Ed. 62 (2023) e202303888.
[48] J. Holoubek, H. Liu, Z. Wu, et al., Nat. Energy 6 (2021) 303–313.
[49] S. Zhong, Y.S. Yu, Y. Yang, et al., Angew. Chem. Int. Ed. 62 (2023) e202301169.
[50] Y. Li, F. Wu, Y. Li, et al., Chem. Soc. Rev. 51 (2022) 4484–4536.
[51] Z. Tian, Y. Zou, G. Liu, et al., Adv. Sci. 9 (2022) 2201207.
[52] S. Wang, X.G. Zhang, Y. Gu, et al., J. Am. Chem. Soc. 146 (2024) 3854–3860.
[53] F.A. Soto, P. Yan, M.H. Engelhard, et al., Adv. Mater. 29 (2017) 1606860.
[54] Y. Wang, H. Li, B. Zhai, et al., ACS Nano 18 (2024) 3456–3467.
[55] J. Bai, J.H. Jia, Y. Wang, et al., Nano-Micro Lett. 17 (2024) 1–16.
[56] H. Liang, L. Liu, N. Wang, et al., Adv. Mater. 34 (2022) 2202873.
[57] M. Li, H. Zhuo, Q. Jing, et al., Carbon Energy 6 (2024) e546.
[58] Z.C. Bai, Q. Yao, M.Y. Wang, et al., Adv. Energy Mater. 14 (2024) 2303788.
[59] Y.H. Feng, M.T. Liu, J.X. Wu, et al., Angew. Chem. Int. Ed. 63 (2024) e202403585.
[60] Y. Li, Y. Yang, Y. Lu, et al., ACS Energy Lett. 5 (2020) 1156–1158.
[61] C. Wu, Y. Yang, Y. Li, et al., Energy Environ. Sci. 18 (2025) 6019–6031.
[62] H.Y. Fang, Y.H. Huang, W. Hu, et al., Angew. Chem. Int. Ed. 63 (2024) e202400539.
[63] H. Chen, C. Zhao, H. Yue, et al., Chin. Chem. Lett. 36 (2025) 109650.
[64] Z. Tang, H. Wang, P.F. Wu, et al., Angew. Chem. Int. Ed. 61 (2022) e202200475.
[65] J. Liu, Z. Ni, C. Wei, et al., Energy Storage Mater. 72 (2024) 103753.
[66] M. Wang, L. Yin, M. Zheng, et al., Nat. Commun. 15 (2024) 8866.
[67] Z. Tian, Y. Zou, G. Liu, et al., Adv. Sci. 9 (2022) 2201207.
[68] C. Yang, X.W. Liu, Y. Lin, et al., Adv. Mater. 35 (2023) 2301817.
[69] Y.Y. Wang, H. Lan, S. Dong, et al., Adv. Funct. Mater. 34 (2024) 2315498.
[70] Y. Cui, Y. Ni, Y. Wang, et al., J. Chen, Adv. Energy Mater. 15 (2025) 2405363.
[71] Z. Wang, T. Zheng, S. Wang, et al., J. Am. Chem. Soc. 147 (2025) 5962–5970.
[72] C. Li, H. Xu, L. Ni, et al., Adv. Energy Mater. 13 (2023) 2301758.
[73] X. Hou, S. Wang, B. Wang, et al., Angew. Chem. Int. Ed. 64 (2025) e202416939.
[74] R. Shao, Z. Sun, L. Wang, et al., Angew. Chem. Int. Ed. 63 (2024) e202320183.
[75] J. Zhou, Y. Ding, Y. Wang, et al., J. Colloid Interface Sci. 657 (2024) 502–510.
[76] C. Zheng, Q. Yao, Y. Sun, et al., Adv. Funct. Mater. (2025), doi:10.1002/adfm.202501303.
[77] L. Deng, K. Goh, F.D. Yu, et al., Energy Storage Mater. 44 (2022) 82–92.
[78] L.M. Yin, M.L. Wang, C. Xie, et al., ACS Appl. Mater. Interfaces 15 (2023) 9517–9523.
[79] Y. Liu, Y. Gong, K. Chen, et al., Adv. Funct. Mater. 34 (2024) 2403138.
[80] Y.T. Liu, H.J. Liang, M. Du, et al., J. Mater. Sci. Technol. 182 (2024) 111–118.
[81] M.X. He, L.J. Zhu, G. Ye, et al., Angew. Chem. Int. Ed. 63 (2024) e20240105.
[82] Q. Yang, X. Zhou, T. Huang, et al., Angew. Chem. Int. Ed. 64 (2025) e202422259.
[83] X. Zhang, Z. Xu, J. Xie, et al., J. Energy Storage 80 (2024) 110263.
[84] Q. Zhang, X. Wang, H. Li, et al., J. Electrochem. Soc. 172 (2025) 010501.
[85] P. Zhou, Z. Zhao, J. Weng, et al., ACS Energy Lett. 10 (2024) 185–194.
[86] L. Que, F. Yu, J. Wu, et al., Proc. Natl. Acad. Sci. U. S. A. 121 (2024) e2311075121.
[87] H.J. Liang, H.H. Liu, X.X. Zhao, et al., J. Am. Chem. Soc. 146 (2024) 7295–7304.
[88] S. Li, H. Liu, H. Qiu, et al., Chem. Eng. J. 505 (2025) 159102.
[89] J. Cai, A. Wang, S. Li, et al., Energy Storage Mater. 75 (2025) 103997.
[90] M. Li, C. Wang, Z. Chen, et al., Chem. Rev. 120 (2020) 6783.
[91] G. Xu, X. Shangguan, S. Dong, et al., Angew. Chem. Int. Ed. 59 (2020) 3400–3415.
[92] M. Xia, H. Chen, Z. Zheng, et al., Adv. Energy Mater. 15 (2024) 2403306.
[93] Y. Shen, J. Xu, Y. Li, et al., J. Mater. Chem. A 12 (2024) 33559–33571.